

A Glycine Derivative as Corrosion Inhibitor for Carbon Steel in 3.5 wt% NaCl solution: The combined Experimental and Theoretical Calculation

Li Chen¹, Yi He^{*2,3}, Qiangbin Yang², RanRan Yang², Liyun Zhang², Yi Fan², Ze He^{*2,3}

¹ School of Pharmacy, Chengdu Medical College, Chengdu, Sichuan, China, 610500

² College of Chemistry and Chemical Engineering, Southwest Petroleum University, 8 Xindu Avenue, Chengdu, Sichuan 610500, China

³ Chengdu SDLTec. Company, Chengdu, Sichuan, China, 610500

*E-mail: heyi@swpu.edu.cn, heze1313@hotmail.com

Received: 20 November 2017 / Accepted: 8 March 2018 / Published: 10 April 2018

A novel glycine derivative, (9H-fluoren-9-yl) methyl (2-(heptadecyl amino)-2-oxoethylcarbamate (FMOC), was synthesized and investigated as a corrosion inhibitor for N80 carbon steel in a 3.5% sodium chloride solution using weight loss measurements, potentiodynamic polarization, and electrochemical impedance spectroscopy (EIS). The surfaces of the corrosive steels were studied with scanning electron microscopy (SEM), energy dispersive spectroscopy (EDS), and X-ray photoelectron spectroscopy (XPS). Polarization curves revealed that FMOC acted as a mixed-type inhibitor. The inhibition efficiency increased with increasing FMOC concentration at different temperatures. The adsorption of FMOC on the metal surface is confirmed to involve physisorption and chemisorption. Quantum chemical calculations were performed to explain the mechanism of the interaction between FMOC and the steel surface.

Keywords: Corrosion inhibitor, Glycine derivative, Quantum chemical calculations, Adsorption.

1. INTRODUCTION

Metal corrosion remains a critical issue. Currently, approximately 80 percent of petroleum and chemical equipment is manufactured with iron-carbon alloys. However, these alloys still suffer from poor corrosion resistance. Adding organic inhibitors is an efficient method to protect materials from corrosion. Generally, organic inhibitor molecules contain N, O, and S heteroatoms, which can adsorb on the metal surface by supplying lone electron pairs to the metal[1, 2]. In particular, organic inhibitors containing nitrogen exhibit good corrosion inhibition performance, as their nitrogen atoms can provide plenty of lone electron pairs for the p-orbital character of free electrons and the electron density of the

surrounding atoms [3]. Unfortunately, the commonly used inhibitors are chemical compounds that are harmful to the environment and human health[4, 5]. It comes as a pleasant surprise that the addition of amino acids, or their derivatives, which contain plenty of nitrogen, offer a good anti-corrosion effect without damaging the environment.

Recently, amino acids and derivatives based on corrosion inhibitors have aroused great interest. For example, Fu et al[6] investigated the corrosion inhibition behaviour of four selected amino acid compounds, namely, L-cysteine, L-histidine, L-tryptophan and L-serine, on a mild steel surface in a deaerated 1 M HCl solution. The inhibition effect of alanine, glycine and leucine against steel corrosion in HCl solutions has been investigated by Ashassi-Sorkhabi [7]. A glycine derivative 2-(4-(dimethylamino)benzylamine) acetic acid hydrochloride was used to inhibit uniform and pitting corrosion processes of Al in 0.50 M KSCN solutions in the work of Amin et al [8]. However, little attention has been paid to inhibitors for mild steel in a NaCl-containing environment, and the simple structure of amino acids limited their corrosion efficiency.

Recently, glycine-based, environmentally friendly corrosion inhibitors for metal have been explored by Amin and co-workers [9]. We have synthesized a new, safe, glycine-based inhibitor, a new glycine derivative named (9H-fluoren-9-yl) methyl (2-(octadecylamine)-2-oxoethyl) carbamate (FMOC), to effectively inhibit N80 carbon steel in a 3.5% sodium chloride solution by weight at room temperature. Weight loss measurements, potentiodynamic polarization tests, electrochemical impedance spectroscopy, scanning electron microscopy and X-ray photoelectron spectroscopy were used to evaluate the efficiency and verify the adsorption of the inhibitor. Quantum chemical calculations aimed to find the adsorption mechanism between the inhibitor molecules and the metal surface, intermolecular adsorption, adsorption centre of the inhibitor and electronic properties of the novel glycine derivative. Therefore, quantum chemical calculations mainly calculated the energy of the highest occupied molecular orbital (E_{HOMO}) and the lowest unoccupied molecular orbital (E_{LUMO}), the number of transferred electrons (ΔN) and the Hirshfeld atomic charges on the trunk atoms of the novel glycine derivative corrosion inhibitor.

2. EXPERIMENT

2.1. Pretreatment of the steel sheets

The experiments were performed with N80 carbon steel. The elemental composition of the sample was as follows (wt%): 0.24% C, 0.22% Si, 1.19% Mn, 0.013% P, 0.004% S, 0.015% V, and 0.0036% Cr, and the remainder was Fe. Prior to the experiment, the surface of the steel was polished by mechanical grinding with 400, 800 and 1200 emory paper and then washed in acetone, ethanol, and deionized water.

2.2. Synthesis of FMOC

FMOC was synthesized according to the procedures described below in Fig. 1. The 6 mmol Glycine and 6.3 mmol Fmoc N-hydroxysuccinimide este (Fmoc-OSu) were dissolved in 25 ml N,N-

Dimethylformamide (DMF) with vigorous stirring at room temperature and refluxed for 2 h. Small amounts of anhydrous sodium bicarbonate were used during the process. Finally, the solvents were removed, and the residue was maintained for 12 h under a 50 °C vacuum environment, which obtained the Fmoc-glycine [10]. The 4.42 mmol Fmoc-glycine and 4.42 mmol SOCl₂ were added to 25 ml CH₂Cl₂ at 50 °C and refluxed for 4 h. Then, 4.42 mmol octadecylamine was added to the above mixture and vigorously stirred and refluxed for 24 h at 50 °C. The above process was carried out in a nitrogen gas environment. Finally, the FMOC was isolated by column chromatography.

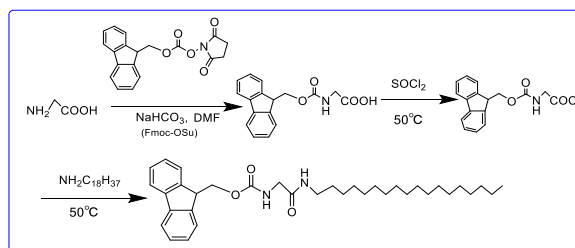


Figure 1. Synthetic route of FMOC

2.3. ¹H NMR spectra determination

The chemical structure of the FMOC was determined by NMR spectroscopy. ¹H NMR spectra were recorded with a Bruker Avance III 400 NMR (Bruker BioSpin, Switzerland) in CDCl₃ at room temperature.

2.4. Weight loss measurements

The prepared specimens of N80 carbon steel were accurately weighed, and the surface area was computed. The corrosive medium was 3.5 wt% sodium chloride aggressive solution. Sodium chloride (AR grade) was purchased from the Kelong Chemical Reagent Factory (Chengdu, China). These specimens were immersed in the 3.5 wt% sodium chloride solution containing a different concentration of inhibitor and maintained at 298 K. After a period of time, the specimens were taken out, washed, dried, and accurately weighed. The average weight loss of the three parallel specimens could be obtained. The inhibition efficiency (η) and the degree of surface coverage (θ) at different concentrations of investigated inhibitor on the corrosion of the specimens were calculated as follows[11]:

$$r_{\text{corr}} = \frac{\Delta m}{ST} \quad (1)$$

$$\eta\% = \frac{r_{\text{corr}}^0 - r_{\text{corr}}}{r_{\text{corr}}^0} \times 100 \quad (2)$$

$$\theta = \frac{r_{\text{corr}}^0 - r_{\text{corr}}}{r_{\text{corr}}^0} \quad (3)$$

Where Δm is the average weight loss of the three parallel specimens. S and T are the area of metal surface and immersing time in corrosive solution, respectively. Subsequently, r_{corr}^0 and r_{corr} represent the corrosion rate without and with FMOC inhibitor, separately.

2.5. Electrochemical experiments

An electrochemical work station, including a computer-controlled system (CorrTest Company, Wuhan, China) and a conventional three-electrode compartment, were employed in the experiment. The N80 carbon steel was used as a working electrode (WE), along with a platinum counter electrode as the auxiliary electrode (AE) and a saturated calomel electrode (SCE) as the reference electrode (RE). Before EIS and polarization measurement, the working electrode was immersed in aggressive medium for 30 min to obtain a stable open circuit potential (OCP); the corrosive medium was a 3.5 wt% sodium chloride solution containing a different concentration of inhibitor and maintained at 298 K.

2.5.1 Polarization measurements

The polarization measurements were conducted in a potential range from -0.75 to -0.25 V vs SCE with a scanning rate of 1 mV s⁻¹. The linear Tafel segments of the anodic and cathodic curves were extrapolated to the corrosion potential (E_{corr}) to obtain the corrosion current density (i_{corr}). The inhibition efficiency $\eta_p(\%)$ and surface coverage (θ) were determined by Eqs. (4) and (5) [12,13].

$$\eta_p(\%) = \frac{i_{\text{corr}}^0 - i_{\text{corr}}}{i_{\text{corr}}^0} \times 100 \quad (4)$$

$$\theta = \frac{i_{\text{corr}}^0 - i_{\text{corr}}}{i_{\text{corr}}^0} \quad (5)$$

2.5.2. EIS measurements

EIS tests were conducted at the OCP at a frequency from 100 kHz to 0.01 Hz at an alternating current amplitude of 5 mV. ZSimpWin software was carried to analyse the impedance data. The inhibition efficiency $\eta_z(\%)$ was calculated by the following Eq. (6) [13]:

$$\eta_z(\%) = \frac{R_{\text{ct}} - R_{\text{ct}}^0}{R_{\text{ct}}} \times 100 \quad (6)$$

where R_{ct}^0 and R_{ct} represent the charge transfer resistances in the corrosive medium without and with different concentrations of inhibitor, respectively.

The Kramers-Kronig transformation (KKT) was performed to confirm the validity of the impedance data. KKTs are integral equations that constrain the real and imaginary components of the

complex quantities for the systems, which satisfy four basic conditions, including Linearity, Causality, Stability and Finiteness. The corresponding equations are written as Eqs. (7) and (8)[14].

$$Z'(\omega) = Z'(\infty) - \frac{2}{\pi} \int_0^{\infty} \frac{xZ'' - \omega Z''(\omega)}{x^2 - \omega^2} dx \quad (7)$$

$$Z''(\omega) = -\frac{2\omega}{\pi} \int_0^{\infty} \frac{Z'(x) - Z'(\omega)}{x^2 - \omega^2} dx \quad (8)$$

where ω is the frequency of transformation, x is the frequency of integration, and Z' and Z'' are the real and imaginary impedance components, respectively. Eq. (7) provides an imaginary axis-to-real axis transformation, while Eq. (8) represents the real axis-to-imaginary axis transformation, and the average error (η) was also calculated with Eq. (9)[14].

$$\eta \% (Z) = \frac{100 \sum |Z_{ex}(\omega) - Z_{KKT}(\omega)|}{NZ_{ex,max}} \quad (9)$$

where $Z_{ex}(\omega)$ and $Z_{KKT}(\omega)$ are the values for the real or imaginary part obtained with experimental data and calculated by the appropriate KKT, respectively; $Z_{ex,max}$ is the maximum value of the real or imaginary part in the data, and N is the total number of real/imaginary pairs.

2.6. Scanning electron microscope (SEM)

To investigate the morphology, the specimens were treated in 3.5 wt% NaCl solution without or with 150 mg · L⁻¹ FMOc at 298 K for 72 hours, followed by washing with water under ultrasound guidance for a minute and placement into a dryer. Then, they were scanned by a scanning electron microscope (JSM-7500F).

2.7. X-ray photoelectron spectroscopy (XPS)

The steel samples were treated with the same procedure as the SEM test. These samples were characterized by X-ray photoelectron spectroscopy (KRATOS, XSAM800).

2.8. Theoretical calculations

Calculation Method: Gaussian 09 D.01 program. The track graph was drawn by Multiwfn+VMD. Geometry optimization, track energy calculation, and Hirshfeld charge analysis were performed using B3LYP-D3 (BJ) functional binding with the 6-311G * basis set (for C, O, N) and 6-31G * basis set (for H).

3. RESULTS AND DISCUSSION

3.1. The spectrum of ^1H NMR

The ^1H NMR test for FMOC was conducted in CDCl_3 . As shown in Fig. 2, the signals of H at 7.81 ppm, corresponding to NH protons, confirm that FMOC was synthesized.

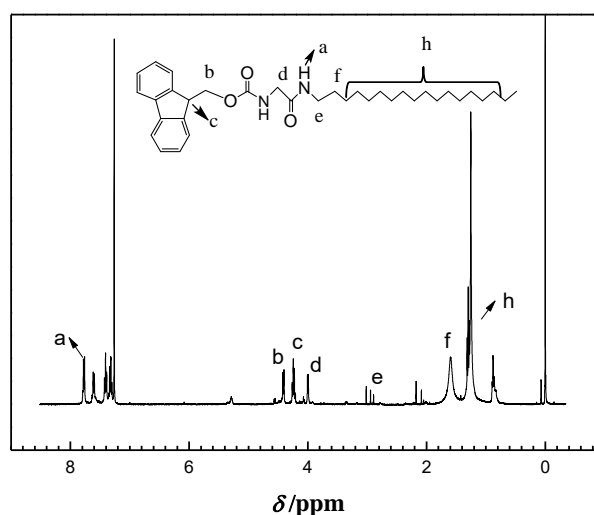


Figure 2. ^1H NMR spectra of FMOC in CDCl_3

3.2. Weight loss studies

Table 1. The parameters for weight loss experiment of N80 carbon steel at different times in 3.5 wt% NaCl solution containing various concentrations of FMOC at 298 K.

Time (h)	C ($\text{mg}\cdot\text{L}^{-1}$)	Δm (mg)	S (cm^2)	r_{corr} ($\text{g}\cdot\text{cm}^{-2}\cdot\text{h}^{-1}$)	η (%)	θ (%)
36 h	0	0.0163	6.7968×10^{-3}	0.6662	-	-
	50	0.0082	6.7469×10^{-3}	0.3362	49.54	0.4954
	100	0.0058	6.7891×10^{-3}	0.2352	64.69	0.6469
	150	0.0040	6.7971×10^{-3}	0.1633	75.48	0.7548
	200	0.0019	6.7608×10^{-3}	0.0760	88.59	0.8859
72 h	0	0.0212	6.7862×10^{-3}	0.6507	-	-
	50	0.0104	6.7466×10^{-3}	0.3210	50.66	0.5066
	100	0.0072	6.8055×10^{-3}	0.2191	66.32	0.6632
	150	0.0049	6.8336×10^{-3}	0.1502	76.92	0.7692
	200	0.0024	6.7739×10^{-3}	0.0729	88.79	0.8879
108 h	0	0.0468	6.7086×10^{-3}	0.6455	-	-
	50	0.0218	6.7321×10^{-3}	0.2990	53.68	0.5368

	100	0.0151	6.7754×10^{-3}	0.2058	68.12	0.6812
	150	0.0108	6.7856×10^{-3}	0.1465	77.31	0.7731
	200	0.0052	6.7470×10^{-3}	0.0716	88.90	0.8890
144 h	0	0.0622	6.8269×10^{-3}	0.6325	-	-
	50	0.0281	6.7515×10^{-3}	0.2908	54.03	0.5403
	100	0.0192	6.7525×10^{-3}	0.1972	68.82	0.6882
	150	0.0139	6.7624×10^{-3}	0.1425	77.48	0.7748
	200	0.0069	6.7640×10^{-3}	0.0710	88.78	0.8878

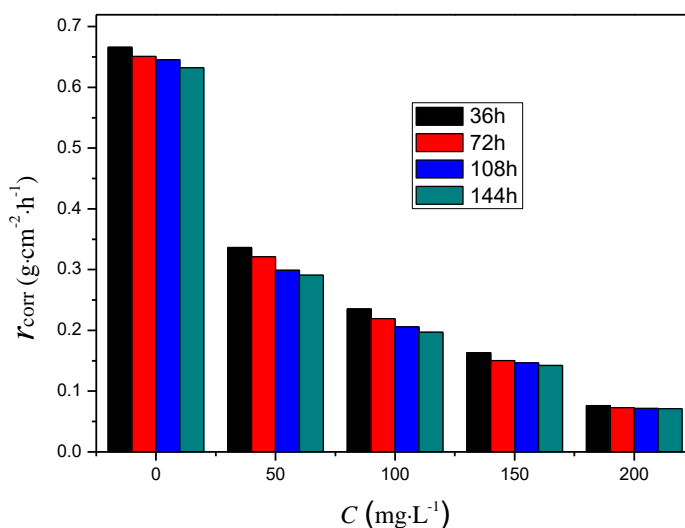


Figure 3. Corrosion rate (r_{corr}) for N80 carbon steel for different times in 3.5 wt% NaCl solution containing various concentrations of FMOC at 298 K.

Table 1 shows the weight loss results of N80 carbon steel in 3.5 wt% NaCl solution for different periods with different concentrations of inhibitor. It can be found that the inhibition efficiency of the FMOC inhibitor increased with increasing inhibitor concentrations, and the value of η can be above 88% for different periods when the concentration of inhibitor reached $200 \text{ mg}\cdot\text{L}^{-1}$. This result demonstrated that inhibitor molecules of FMOC better protect the metal surface at higher concentrations. The obtained r_{corr} was determined in Fig. 3, in which the value of r_{corr} decreased with increasing concentrations of inhibitor. In addition, the value of r_{corr} was lower for a longer time, and this change became obvious at the concentration of $200 \text{ mg}\cdot\text{L}^{-1}$. This can be attributed to the protective role of corrosion products in addition to the protection of the inhibitor, since large areas of corrosion were found in the carbon steel when the inhibitor was absent or at low concentration in the solution. The corrosion in the higher concentration of FMOC would be mainly restrained by inhibitory molecules, so the r_{corr} had no obvious change at the concentration of $200 \text{ mg}\cdot\text{L}^{-1}$.

3.3. Potentiodynamic polarization tests

The effect of FMOC on the polarization behaviour of N80 carbon steel was studied by potentiodynamic polarization experiments. Potentiodynamic polarization for different concentrations of FMOC at different temperatures in 3.5 wt.% NaCl were carried out, and the obtained cathodic and anodic polarization curves of the carbon steel electrodes are shown in Fig. 4. The parameters, such as corrosion potential (E_{corr}), corrosion current density (i_{corr}) and anodic (β_a)/cathodic (β_c) Tafel slopes, were obtained from the extrapolation of the polarization curves and are presented in Table 2.

It can be seen from Fig. 4 that the anodic polarization curves moved to the left compared with the blank, and the obtained anodic Tafel slope values became smaller, indicating that the anodic reaction of steel corrosion was distinctly suppressed after adding to the inhibitor. Additionally, the cathodic Tafel slope values had more obvious increases in the presence of the inhibitor, confirming that the cathodic reaction of carbon steel corrosion was significantly inhibited in the presence of the inhibitor. In Table 2, comparing the E_{corr} of the blank test, the change in the E_{corr} value of other concentrations was not over 85 mV, and the change of largest value was 46 mV. Usually, the inhibitor can be classified as a cathodic or anodic type when the change in the value of the corrosion potential (E_{corr}) is larger than 85 mV[15]. Thus, it can be inferred that FMOC acted as a mixed-type inhibitor. In addition, the cathodic Tafel slope values had a more obvious change than the anodic Tafel slope values in the presence of the inhibitors. This indicated that the FMOC acted as a mixed-type inhibitor to predominantly inhibit the cathodic reaction of the mild steel in 3.5 wt.% NaCl solution. In fact, all these inhibitors exhibit stronger inhibitive effects on the cathodic reaction than on the anodic reaction[16].

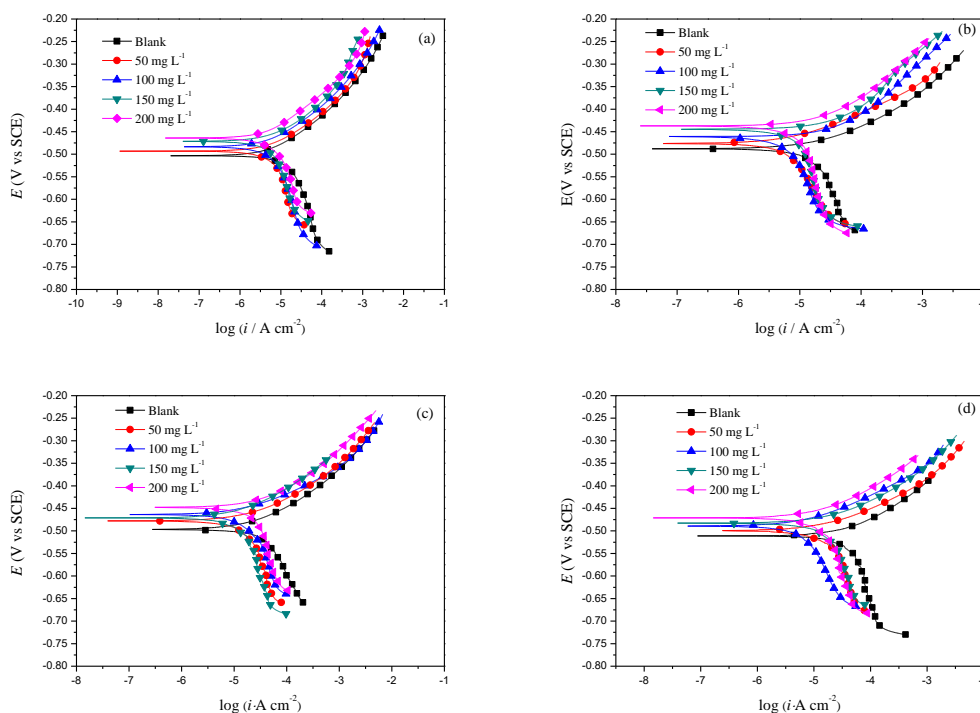


Figure 4. Potentiodynamic polarization curves for N80 carbon steel in 3.5 wt.% NaCl solution containing various concentrations of FMOC at different temperatures (a) 298 K, (b) 308 K, (c) 318 K, (d) 328 K

From Table 2, the value of θ was shown to be increased with the increase of the concentration of FMOC at the same temperature, which revealed that the increased concentration of the inhibitor accelerated the efficient and extensive FMOC adsorption on the metal surface. Furthermore, the decreased value of θ decreased by increasing temperature at the same concentration of inhibitor, demonstrating that a higher temperature results in the desorption of the originally adsorbed FMOC molecule from the surface of metal.

Table 2. The electrochemical kinetic parameters for the polarization curves of N80 carbon steel in 3.5 wt.% NaCl solution containing various concentrations of FMOC at different temperatures.

T (K)	C ($\text{mg}\cdot\text{L}^{-1}$)	E_{corr} (mV vs SCE)	β_{c} ($\text{mV}\cdot\text{dec}^{-1}$)	β_{a} ($\text{mV}\cdot\text{dec}^{-1}$)	i_{corr} ($\text{mA}\cdot\text{cm}^{-2}$)	η_{p} (%)	θ (%)
298	0	-502	-556	120	0.1468	--	--
	50	-483	-497	117	0.0685	53.34	0.5334
	100	-469	-478	109	0.0419	71.46	0.7146
	150	-452	-462	97	0.0287	80.45	0.8045
	200	-446	-449	86	0.0153	89.58	0.8958
308	0	-489	-568	136	0.3125	--	--
	50	-473	-512	124	0.1554	50.27	0.5027
	100	-458	-494	112	0.1021	67.33	0.6733
	150	-453	-489	105	0.0683	78.14	0.7814
	200	-449	-478	98	0.0382	87.78	0.8778
318	0	-483	-518	132	0.5739	--	--
	50	-469	-496	127	0.2893	49.59	0.4959
	100	-451	-487	128	0.2011	64.96	0.6496
	150	-448	-479	114	0.1432	75.05	0.7505
	200	-441	-471	108	0.0779	86.43	0.8643
328	0	-493	-504	142	0.7432	--	--
	50	-488	-484	131	0.3934	47.07	0.4707
	100	-473	-478	118	0.2761	62.85	0.6285
	150	-469	-465	105	0.1965	73.56	0.7356
	200	-464	-456	108	0.1112	85.04	0.8504

3.4. Electrochemical impedance spectroscopy (EIS)

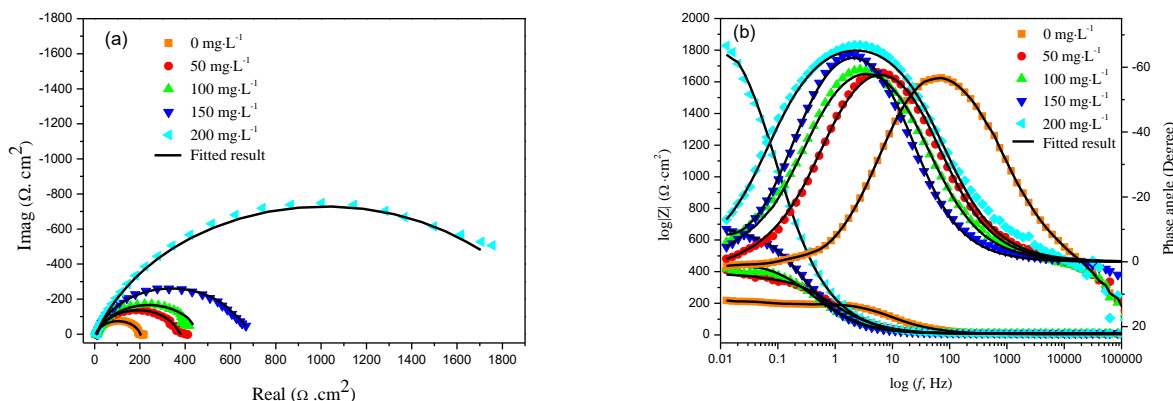


Figure 5. Nyquist plots and Bode plots of N80 carbon steel in 3.5 wt% NaCl solution containing different concentrations of FMOC at 298 K; (a) Nyquist plots, (b) Bode plots.

The effect of the inhibitor concentration on N80 carbon steel was studied using EIS measurements in 3.5 wt% NaCl medium in different concentrations of FMOC at 298 K. Nyquist plots and Bode plots are shown in Fig. 5, and the corresponding real-to-imaginary and imaginary-to-real KKT data was shown in Fig. 6. The values of $\eta_z/\%$ in transforming the experimental data by KKTs at 298 K are shown in Table 3. It can be seen from Fig. 6 (a and b) and Table 3 that the value of $\eta_z/\%$ in all the FMOC concentrations is reasonable. Therefore, there is relative agreement between the experimental EIS and KKT data, suggesting that the experimental EIS data fit with the KKTs.

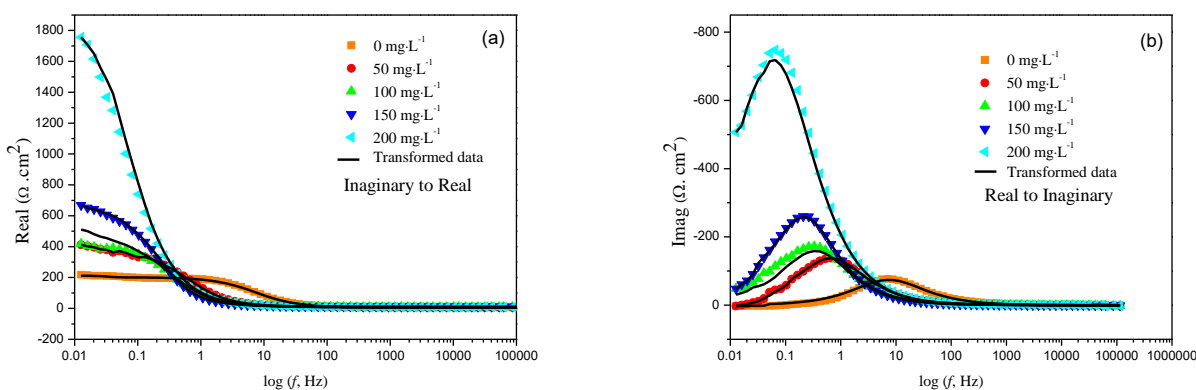


Figure 6. Comparison of the experimental EIS data and KKT data of steel in 3.5 wt% NaCl solution containing different concentrations of FMOC at 298 K.

Table 3. Values of $\eta_z/\%$ in transforming the experimental data by KKTs.

$C/\text{mg}\cdot\text{L}^{-1}$	0	50	100	150	200
Z'	0.6625	0.7768	0.03264	0.08675	4.7880
Z''	2.5674	0.6364	0.3562	5.461	3.175

As shown in Fig. 5, with the increase of the FMOC concentration, the semi-circular loop of impedance becomes enlarged. There is a similarity between the shapes of electrochemical impedance plots for the inhibited electrodes and uninhibited electrodes in all cases. This revealed that adding inhibitors only changed the impedance values but did not alter the other impedance performance. It is obvious that total Nyquist plots and Bode plots are presented in a single capacitive loop, which indicate that, during the course of metal dissolution, there was only one charge transfer reaction[17], which excluded the other processes in the whole frequency range.

An equivalent circuit model (Fig. 7) with a constant phase element (CPE) was employed to analyse the impedance spectra, and the fitted results are shown in Fig. 5. The component R_s represents the solution resistance; R_{ct} represents the charge transfer resistance; and Q_{dl} represents the CPE of electric double layer capacitance, with the relevant parameters listed in Table 4. The impedance of CPE was calculated using Eq.(10) [18]:

$$Z_{CPE} = Y_0^{-1}(j\omega)^{-n} \quad (10)$$

where Y_0 and n are the CPE constant, ω is the angular frequency ($\omega = 2\pi f$) when $-Z''$ at wave crest, j is the imaginary number, and n can be used to comprehend the extent of the surface roughness during the formation of the multilayer[19].

It can be concluded from Table 4 that the presence of FMOC in aggressive medium led to a decrease in the Q_{dl} values. The decrease of Q_{dl} can be attributed to the decrease of the local dielectric constant and an increase in the thickness of the electrical double layer after adding FMOC[15]. Meanwhile, the increase in R_{ct} is due to the formation of a protective film on the electrode surface through the adsorption of organic molecules, which gradually replace the water molecules at the metal/solution interface after decreasing the degree of the dissolution reaction[20]. In addition, with the rising dosage of FMOC, an increasing inhibition efficiency ($\eta_z\%$) of 90.24% is an outcome of the R_{ct} increase. Obviously, the inhibition efficiency values gained by the impedance method (Table 4) are consistent with those values from the results of the weight loss (Table 1) and polarization technique (Table 2).

Table 4. Electrochemical impedance parameters for N80 steel electrodes in the absence and presence of FMOC

$C/\text{mg}\cdot\text{L}^{-1}$	$R_s/(\Omega\cdot\text{cm}^2)$	$Y_0/(\text{S s}^n \text{cm}^{-2})$	n	$R_{ct}/(\Omega\cdot\text{cm}^2)$	$Q_{dl}/(\mu\text{F}\cdot\text{cm}^{-2})$	$\eta_z/\%$	θ
0	5.38	223.1	0.81	197.8	107		
50	8.37	191.5	0.81	370.0	102	46.54	0.4654
100	8.73	170.7	0.81	464.4	94	57.41	0.5741
150	11.55	126.9	0.81	651.6	71	69.64	0.6964
200	7.426	99.00	0.81	2026.0	67	90.24	0.9024

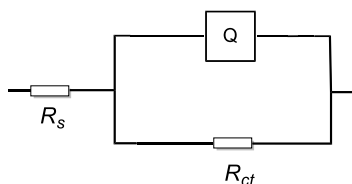
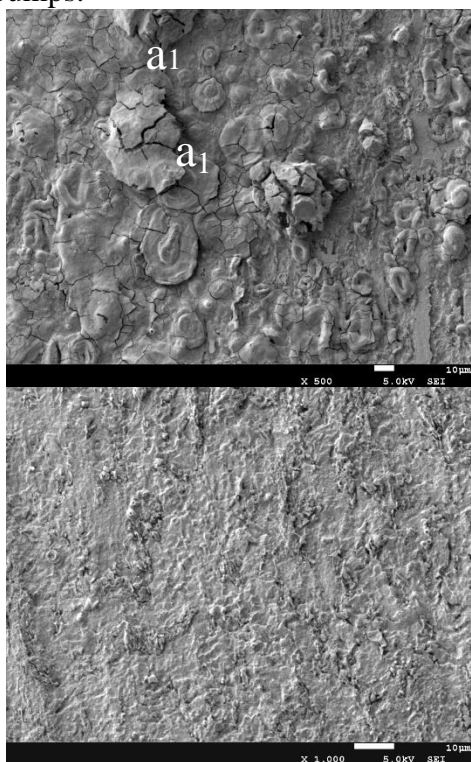


Figure 7. Fitted equivalent circuit diagram

3.5. N80 carbon steel surface morphological and element analysis

After immersion for 72 hours in aggressive medium, the surface of the steel was investigated by scanning electron microscopy (SEM). As shown in Fig. 8, the carbon steel surface without inhibitor had some bumps, and the surface in $150 \text{ mg} \cdot \text{L}^{-1}$ inhibitor was relatively flat. The two surfaces were further detected by energy dispersive spectroscopy (EDS), and the percentage of corresponding atoms are displayed in Table 5. We found that the oxygen atom content of the blank was significantly higher, which indicated that more corrosion occurred. In addition, the charged ions easily passed the loosened corrosion product films in the corrosion cells[21], which would result in localized corrosion, and the surface of blank steel had some bumps.



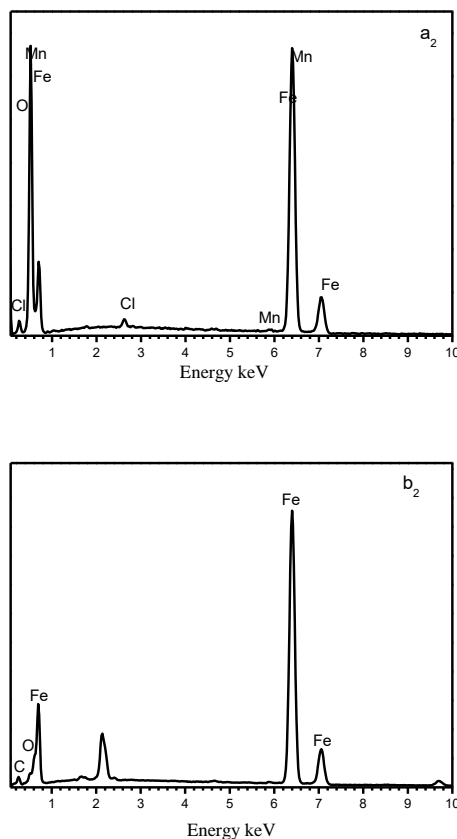


Figure 8. SEM and EDS of N80 steel after immersion for 72 hours in aggressive medium: uninhibited (a_1, a_2) and inhibited (b_1, b_2) by $150 \text{ mg} \cdot \text{L}^{-1}$ of FMOC

Table 5. The percentage of the atoms on the uninhibited and inhibited N80 steel surface by EDS

Atomic (%)	C	O	Fe	Mn	Cl
Blank	13.72	59.17	26.55	0.30	0.40
$150 \text{ mg} \cdot \text{L}^{-1}$ FMOC	25.10	6.98	67.92	--	--

The XPS was also used to study the surface of the carbon steel. The adsorption of the FMOC was studied with the characteristic C1s and N1s peak signals. The deconvoluted profiles of C1s and N1s are presented in Fig. 9. Three decomposed peaks (Fig. 9a) of C1s suggest that there are three chemical forms on the glycine derivative structure. Binding energy of 284.8 eV can be assigned to the C-C aromatic bonds, and the peak at 285.5 eV may be resulted from the C-N bonds. The peak of 288.4 eV may be attributed to the carbon in C=O and N-C=O bonds [22]. The N1s spectrum was fitted to three peaks centred at 398.8, 400.3, and 402.0 eV, which corresponded to N-Fe, N-C and NH-C=O bands, respectively (Fig. 9b). The obtained XPS result exhibits almost same characteristic bands of the glycine derivative molecule, which confirmed that the inhibitor was adsorbed on the steel samples.

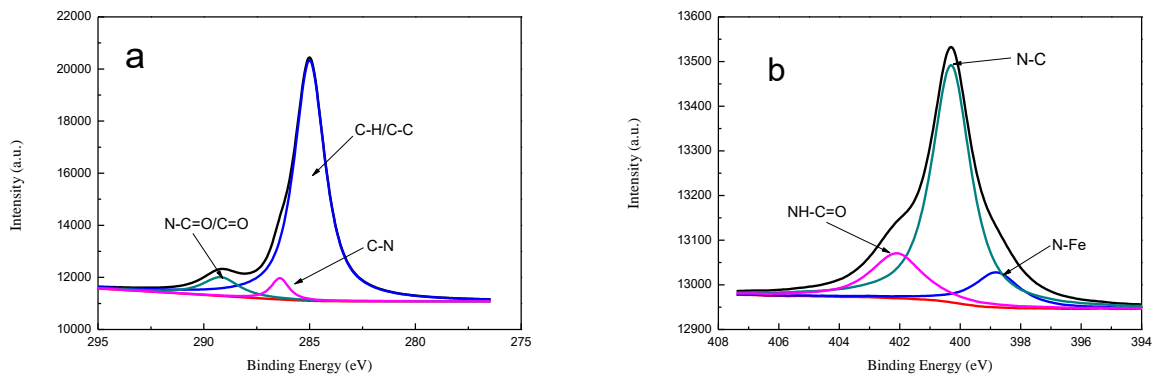


Figure 9. C1s and N1s spectra for the inhibitor molecule-treated N80 carbon steel

3.6. Adsorption isotherm

Adsorption isotherms were employed to describe the basic information on the interaction between the inhibitor and the metal surface. There are three models: Langmuir, Temkin and Frumkin adsorption isotherm[23], which are fitted by the followings equations (11), (12) and (13):

$$\text{Langmuir: } \frac{\theta}{(1 - \theta)} = K_{ads}C_i \quad (11)$$

$$\text{Temkin: } \log\left(\frac{\theta}{C_i}\right) = \log K_{ads} - g\theta \quad (12)$$

$$\text{Frumin: } \log\left(\frac{\theta}{(1 - \theta)C_i}\right) = \log K_{ads} + g\theta \quad (13)$$

where θ is the surface coverage listed in Table 1, which is determined by the i_{corr} , K_{ads} is the adsorption-desorption equilibrium constant, C_i is the concentration of inhibitor and g is the adsorbate interaction parameter. The best fit was obtained with the Temkin adsorption isotherm, as shown in Fig. 10. The linear correlation coefficients (R^2) are close to 1, which are listed in Table 5. This indicated that the adsorption of FMOC obeyed the Temkin adsorption, and K_{ads} is employed to evaluate the standard Gibbs free energy of the adsorption (ΔG_{ads}^0) through Eq. (14):

$$\Delta G_{ads}^0 = -RT \ln(55.5K_{ads}) \quad (14)$$

where R represents the universal gas constant ($J \cdot K^{-1}$), and T is the temperature (K). The values of ΔG_{ads}^0 under different temperatures were calculated using Eq. (14) and are listed in Table 6. It was found that the obtained values of ΔG_{ads}^0 for FMOC are between -20 and -40 kJ mol^{-1} . The values of ΔG_{ads}^0 around -20 kJ mol^{-1} or lower indicated physisorption, which is the electrostatic interaction between the charged molecules and the charged metal. The values of ΔG_{ads}^0 between -20 and -40 kJ mol^{-1} indicate both physisorption and chemisorption. When the values of ΔG_{ads}^0 are around -40 kJ mol^{-1} or higher, they are regarded as chemisorption, involving the sharing or transfer of electrons from the molecules to the metal surface to form a coordinative interaction [24]. Therefore, it could be concluded that the adsorption of FMOC on the metal surface involved physisorption and chemisorption. Generally, electrostatic interactions between the charged molecules and the charged metal is considered physisorption, and the formation of the coordinate bond between the molecules with

unshared electron pairs and/or π -electrons and the metal with a vacant d-orbital is considered to show chemisorption.[16,25] From the structures of FMOc, it is apparent that the electronegative heteroatoms containing N and O are electron-donating groups, which can adsorb onto the metal surface through coordinate bonds. In addition, some FMOc molecules existed in the forms of cationic molecules due to a protonated $-\text{NH}$ or $-\text{C}=\text{O}$ group, and there was an electrostatic interaction between the cationic molecules and the steel surface, which was negatively charged by the specific adsorption of Cl^- ions.[26]

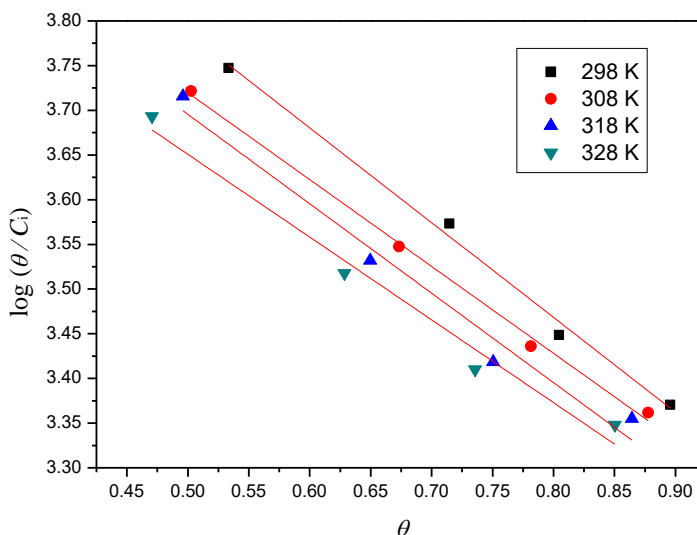


Figure 10. The Temkin adsorption plot of FMOc on N80 steel surface in 3.5 wt.% NaCl solution

Table 6. The values of the standard free energy of adsorption (ΔG_{ads}^0) calculated by Temkin isotherm for FMOc at different temperatures.

Temperature (K)	298	308	318	328
ΔG_{ads}^0 (kJ mol ⁻¹)	-34.58	-35.08	-36.16	-36.78
K_{ads} (M ⁻¹)	2.072×10^4	1.606×10^4	1.569×10^4	1.300×10^4
R^2	0.9915	0.9955	0.9657	0.9691

The transition state equation was employed to evaluate the effect of temperature on the corrosion process as Eq. (15) [1]

$$\ln\left(\frac{i_{\text{corr}}}{T}\right) = \ln\left(\frac{R}{Nh}\right) + \frac{\Delta S^*}{R} - \frac{\Delta H^*}{RT} \quad (15)$$

where N is Avogadro’s number, h is the Planck’s constant, ΔS^* is the entropy of activation, ΔH^* is the enthalpy of activation, R is the general gas constant, and T is the absolute temperature. A plot of $\ln i_{\text{corr}}/T$ versus $1/T$ is shown in Fig. 11. The change in the activation energy E_a of the inhibitor can be regarded as an Arrhenius process and expressed by Eq. (16) [14]:

$$\ln i_{\text{corr}} = -\frac{E_a}{RT} + \ln A \quad (16)$$

where E_a is the apparent activation energy of the corrosion process, and the Arrhenius plots of $\ln i_{\text{corr}}$ versus $1/T$ are presented in Fig. 12. The values of ΔH^* , ΔS^* and E_a are listed in Table 7.

It can be found from Figs. 11 and 12 and Table 7 that the value of E_a and ΔH^* was higher in the presence of the polymer than in the blank solution, which indicated that the introduction of FMOC molecules can inhibit the corrosion reaction in the salt solution by increasing the energy barrier for the corrosion reaction by the adsorption of an active molecule on the metal surface [27,28]. Meanwhile, the values of the entropies (ΔS^*) were found to positively shift in the presence of FMOC, which suggested that the rate determining step for the active complex is an association step rather than a dissociation step, and the decrease in disordering occurs in moving reactants from to the activated complex during the corrosion process [29]. The values of ΔS^* increased with the increase of the FMOC concentration, which was due to the disordered water molecules that were adsorbed on the metal surface and replaced with disordered FMOC molecules.

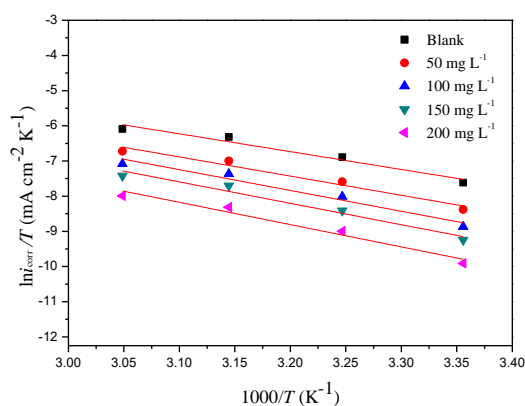


Figure 11. Transition state plots for N80 steel in 3.5 wt% NaCl medium in the absence and presence of different concentrations of FMOC.

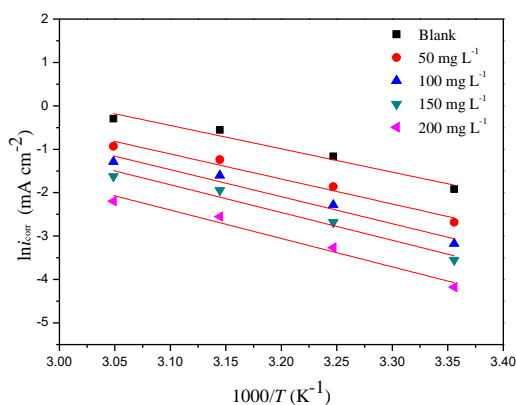


Figure 12. Arrhenius plots for N80 steel in 3.5 wt% NaCl medium in the absence and presence of different concentrations of FMOC.

Table 7. Activation parameters of N80 steel in 3.5 wt% NaCl medium in the absence and presence of different concentrations of FMOC.

C (mg L ⁻¹)	0	50	100	150	200
-------------------------	---	----	-----	-----	-----

$E_a(\text{kJ mol}^{-1})$	44.71	47.90	51.74	53.17	54.40
$\Delta H^*(\text{kJ mol}^{-1})$	42.11	45.30	49.14	50.57	52.63
$\Delta S^*(\text{kJ mol}^{-1} \text{K}^{-1})$	-118.77	-114.35	-105.45	-103.92	-102.37

3.7. Quantum chemical calculations

To investigate the relationship between the molecular electronic structure of FMOc and inhibition performances, quantum chemical calculations were performed. The optimized structure of FMOc is shown in Fig. 13. Quantum chemical parameters, such as E_{HOMO} , E_{LUMO} , ΔE , μ and ΔN , were given in Table 8. Hirshfeld atomic charges of FMOc are shown in Table 9. Furthermore, the orbital density distributions of E_{HOMO} and E_{LUMO} for FMOc are demonstrated in Fig. 14. Based on the frontier orbital theory, E_{HOMO} represents the molecules' electron donating ability, while E_{LUMO} stands for its electron accepting ability. The absolute values of the energy band gap (ΔE) represents the energy to remove an electron from the last occupied orbital[30]. The value of electrons transferred (ΔN) from the inhibitor molecule to the iron atom were calculated by Eq. (17)[31]:

$$\Delta N = \frac{\chi_{\text{Fe}} - \chi_{\text{inh}}}{[2(\eta_{\text{Fe}} + \eta_{\text{inh}})]} \quad (17)$$

where the absolute electronegativity of iron and the inhibitor are represented by χ_{Fe} and χ_{inh} , respectively, and the absolute hardness of the iron and the inhibitor are represented by η_{Fe} and η_{inh} . χ and η can be calculated by the ionization potential (I) and electron affinity (A) in Eqs.(18) and (19) [32]:

$$\chi = \frac{I + A}{2} \quad (18)$$

$$\eta = \frac{I - A}{2} \quad (19)$$

I and A are connected with E_{HOMO} and E_{LUMO} , as shown in Eqs. (20) and (21) [33]:

$$I = -E_{\text{HOMO}} \quad (20)$$

$$A = -E_{\text{LUMO}} \quad (21)$$

The electronegativity of bulk iron is $\chi_{\text{Fe}} \approx 7\text{eV}$, and the overall hardness is $\eta_{\text{Fe}} \approx 0$ in theory. According to Lukovits, the inhibition efficiency increased with the electron donating ability of the inhibitor molecule at the metal surface if $\Delta N < 3.6$ [33]. This was inferred from the value of ΔN in Table 8, and the FMOcs investigated in this study were donors of the electrons, and the iron surface was the acceptor. Furthermore, the orbital density distributions of E_{HOMO} and E_{LUMO} in Fig. 14 were mainly located on the aromatic nucleus, which indicated that these molecules primarily contacted the iron surface.

Table 7. Calculated quantum chemical parameters of FMOc

Total energy (a.u.)	E_{HOMO} (eV)	E_{LUMO} (eV)	ΔE (eV)	μ (Debye)	ΔN
-1700.84	-6.2027	-1.2293	4.9734	3.4627	0.6603

Table 8. Calculated Hirshfeld atomic charges and Fukui functions for FMOC

Atom with numberi ng	atomic charge	f_k^+	f_k^0	f_k^-	Atom with numberi ng	atomic charge	f_k^+	f_k^0	f_k^-
C1	-0.036	0.038	0.036	0.034	O13	-0.254	0.000	0.004	0.007
C2	-0.033	0.058	0.046	0.035	N14	-0.089	0.005	0.009	0.012
C3	0.000	0.048	0.040	0.033	C15	-0.001	0.002	0.008	0.013
C4	0.003	0.029	0.029	0.030	C16	0.151	0.001	0.011	0.022
C5	-0.041	0.048	0.037	0.025	O17	-0.313	0.014	0.050	0.086
C6	-0.039	0.083	0.073	0.063	N18	-0.089	-0.001	0.016	0.032
C7	-0.016	0.007	0.007	0.007	C19	-0.038	0.056	0.046	0.036
C8	0.001	0.030	0.030	0.030	C20	-0.036	0.037	0.036	0.035
C9	-0.004	0.045	0.042	0.039	C21	-0.033	0.078	0.070	0.063
C10	0.037	0.006	0.006	0.005	C22	-0.039	0.046	0.034	0.023
O11	-0.133	0.004	0.006	0.008	C23	-0.033	0.001	0.004	0.008
C12	0.226	0.000	0.002	0.003	C24	-0.039	0.001	0.003	0.005

The Hirshfeld atomic charges of FMOC from Table 9 indicated that C4, C8, C10, C12 and C16 atoms exhibit positive charges, while others exhibit negative charges. In general, the adsorption of the inhibitor molecular occurred on the metal surface through the negative charged atoms of the inhibitor that interacted with the positive charged surface of the metal. The steel surface is positively charged owing to the dissolution of the metal[34-36]. From the result of the frontier molecular orbital density distribution of FMOC, these negatively charged atoms, such as C1, C2, C5, C6, C19, C20, C21, and C22, were first adsorbed on the metal surface. Therefore, the first inhibitor layer was formed on the iron surface. In addition, the higher negative charges were detected on O11, O13, N14, O17 and N18. In the literature[35,37], researchers suggest that there are intermolecular interactions between the negatively and positively charged atoms. Therefore, the other inhibitor molecules in the medium can be accumulated in the first layer by an intermolecular interaction. This means that multilayer inhibition may occur on the metal surface.

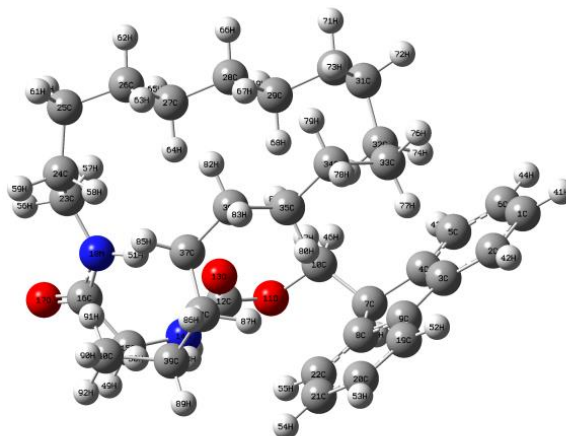


Figure 13. Optimized structures of FMOc

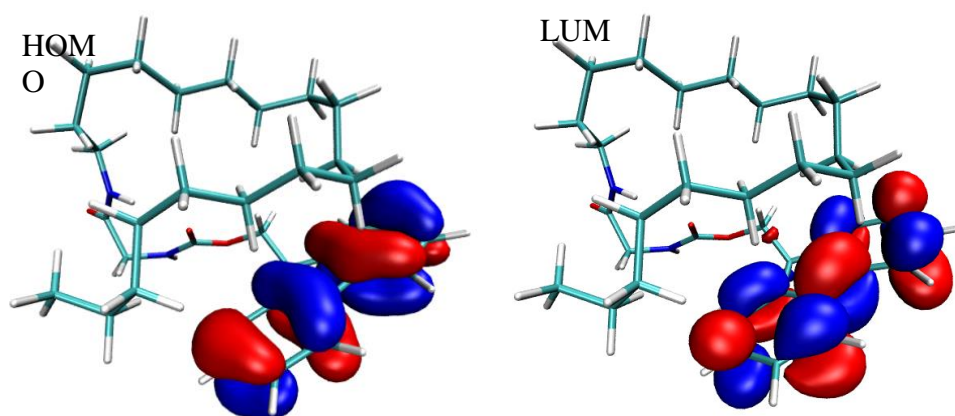


Figure 14. The frontier molecular orbital density distribution of FMOc

4. CONCLUSION

A novel glycine derivative was evaluated as an inhibitor for N80 steel in 3.5 wt.% sodium chloride solution at room temperature. The inhibition efficiency was found to increase with increasing FMOc concentration in the tested experiments. Polarization curves revealed that FMOc acted as a mixed-type inhibitor. The results of SEM, EDS and XPS illuminated that FMOc forms a protective film on the N80 carbon steel surface. A thermodynamics study on evaluating the value of ΔG_{ads}^0 revealed that the FMOc reacted with the metal surface mainly through chemisorption and physisorption. E_{HOMO} , E_{LUMO} and ΔN calculations revealed that the FMOc was an electron donor to the iron surface. The Hirshfeld atomic charges of FMOc showed that the negatively charged atoms of the aromatic nucleus primarily contacted the iron surface and formed a multilayer with intermolecular interactions between the negatively and positively charged atoms.

ACKNOWLEDGEMENTS

This work was financially supported by the Youth Science and Technology Creative Group Fund of Southwest Petroleum University (2015CXTD03) and the Majorly Cultivated Project of Sci-tech Achievements Transition (15CZ0005) from the Education Department in Sichuan Province.

References

1. I. Ahamad, R. Prasad and M.A. Quraishi, *J. Solid State Electrochem.*, 14 (2010) 2095.
2. G. Moretti, F. Guidi and F. Fabris, *Corros. Sci.*, 76 (2013) 206.
3. M. Şahin, G. Gece, F. Karcı and S. Bilgiç, *J. Appl. Electrochem.*, 38 (2008) 809.
4. H. Ashassi-Sorkhabi and M. Es'haghi, *J. Solid State Electrochem.*, 13 (2008) 1297.
5. A.S. Fouda, H.A. Mostafa and H.M. El-Abbasy, *J. Appl. Electrochem.*, 40 (2009) 163.
6. J.-j. Fu, S.-n. Li, Y. Wang, L.-h. Cao and L.-d. Lu, *J. Mater. Sci.*, 45 (2010) 6255.
7. H. Ashassi-Sorkhabi, M.R. Majidi and K. Seyyedi, *Appl. Surf. Sci.*, 225 (2004) 176.
8. M.A. Amin, K.F. Khaled, Q. Mohsen and H.A. Arida, *Corros. Sci.*, 52 (2010) 1684.
9. M.A. Amin, K.F. Khaled and S.A. Fadel-Allah, *Corros. Sci.*, 52 (2010) 140.
10. M.R. Carrasco, R.T. Brown, I.M. Serafimova, and O. Silva, *The Journal of organic chemistry*, 68 (2003) 195.
11. N.A. Negm, N.G. Kandile, E.A. Badr and M.A. Mohammed, *Corros. Sci.*, 65 (2012) 94.
12. F. Zhang, Y. Tang, Z. Cao, W. Jing, Z. Wu and Y. Chen, *Corros. Sci.*, 61 (2012) 1.
13. A. Kosari, M.H. Moayed, A. Davoodi, R. Parvizi, M. Momeni, H. Eshghi and H. Moradi, *Corros. Sci.*, 78 (2014) 138.
14. M. Abdeli, N. Parvini Ahmadi and R. Azari Khosroshahi, *J. Solid State Electrochem.*, 15 (2010) 1867.
15. P.M. Krishnegowda, V.T. Venkatesha, P.K.M. Krishnegowda and S.B. Shivayogiraju, *Ind. Eng. Chem. Res.*, 52 (2013) 722.
16. Y. Tang, F. Zhang, S. Hu, Z. Cao, Z. Wu and W. Jing, *Corros. Sci.*, 74 (2013) 271.
17. C.M.A. BREI-I, *Corros. Sci.*, 33 (1992) 203.
18. S. Javadian, A. Yousefi and J. Neshati, *Appl. Surf. Sci.*, 285 (2013) 674.
19. G. Kear, H.-Z. Wú, M.S. Jones and F.C. Walsh, *J. Appl. Electrochem.*, 38 (2008) 1599.
20. C. Bataillon and S. Brunet, *Electrochim. Acta*, 39 (1994) 455.
21. G.A. Zhang and Y.F. Cheng, *Electrochim. Acta*, 56 (2011) 1676.
22. M. Chevalier, F. Robert, N. Amusant, M. Traisnel, C. Roos and M. Lebrini, *Electrochim. Acta*, 131 (2014) 96.
23. M.W.S. Jawich, G.A. Oweimreen and S.A. Ali, *Corros. Sci.*, 65 (2012) 104.
24. A.M. Atta, O.E. El-Azabawy, H.S. Ismail and M.A. Hegazy, *Corros. Sci.*, 53 (2011) 1680.
25. D. Özkır, K. Kayakırılmaz, E. Bayol, A.A. Gürten and F. Kandemirli, *Corros. Sci.*, 56 (2012) 143.
26. N.A. Negm, N.G. Kandile, E.A. Badr and M.A. Mohammed, *Corros. Sci.*, 65 (2012) 94.
27. A. Singh, I. Ahamad, V.K. Singh and M.A. Quraishi, *J. Solid State Electrochem.*, 15 (2010) 1087.
28. S. Kumar, D. Sharma, P. Yadav and M. Yadav, *Ind. Eng. Chem. Res.*, 52 (2013) 14019.
29. S. Tu, X. Jiang, L. Zhou, M. duan, H. Wang and X. Jiang, *Corros. Sci.*, 65 (2012) 13.
30. G. Gece and S. Bilgiç, *Corros. Sci.*, 51 (2009) 1876.
31. K.F. Khaled, M.N.H. Hamed, K.M. Abdel-Azim and N.S. Abdelshafi, *J. Solid State Electrochem.*, 15 (2010) 663.
32. I.B. Obot and N.O. Obi-Egbedi, *Corros. Sci.*, 52 (2010) 198.
33. O. Olivares, N. Likhanova, B. Gomez, J. Navarrete, M. Llanos-Serrano, E. Arce and J. Hallen, *Appl. Surf. Sci.*, 252 (2006) 2894.
34. S. Martinez, *Mater. Chem. Phys.*, 77 (2002) 97.
35. T. Arslan, F. Kandemirli, E.E. Ebenso, I. Love and H. Alemu, *Corros. Sci.*, 51 (2009) 35.
36. K. Sayin and D. Karakaş, *Corros. Sci.*, 77 (2013) 37.
37. B.D. Mert, A.O. Yüce, G. Kardaş and B. Yazıcı, *Corros. Sci.*, 85 (2014) 287.

© 2018 The Authors. Published by ESG (www.electrochemsci.org). This article is an open access article distributed under the terms and conditions of the Creative Commons Attribution license (<http://creativecommons.org/licenses/by/4.0/>).